# Supplementary Material

## Monolayer $Sc_2NF_2$ and $Sc_2NO_2$ electrodes for bilayer $MoS_2$: Achieving symmetric and excellent performances

Hong Li[1, *], Xiaotian Hu[1], Pengyang Liu[2], Fengbin Liu[1], and Jing Lu[3, 4, 5*]

[1] College of Mechanical and Material Engineering, North China University of Technology, Beijing 100144, P. R. China

[2]Brunel London School North China University of Technology, North China University of Technology, Beijing 100144, P. R. China

[3] State Key Laboratory of Mesoscopic Physics and Department of Physics, Peking University, Beijing 100871, P. R. China

[4] Collaborative Innovation Center of Quantum Matter, Beijing 100871, P. R. China

[5] Peking University Yangtze Delta Institute of Optoelectronics, Nantong 226000, P. R. China

*Corresponding author: jinglu@pku.edu.cn; lihong@ncut.edu.cn

**Table S1**. Parameters of candidate MXene electrodes: metal's lattice parmeter and work function; the supercell of BL $MoS_2$/MXene heterojunction and lattice mismatch on metal layer.

| Interface | Lattice parameter (Å) | mismatch (%) | Supercell ($MoS_2$/ML metal) | Work function (eV) |
|---|---|---|---|---|
| BL $MoS_2/Sc_2NF_2$ | 3.217 | 0 | $1\times1/1\times1$ | -4.07 |
| BL $MoS_2/Sc_2NO_2$ | 3.256 | -1.19 | $1\times1/1\times1$ | -7.62 |
| BL $MoS_2/Ti_2CF_2$ | 3.069 | 4.82 | $1\times1/1\times1$ | -5.21 |
| BL $MoS_2/Ti_2NF_2$ | 3.075 | 4.6 | $1\times1/1\times1$ | -4.87 |
| BL $MoS_2/Zr_2CF_2$ | 3.313 | -2.89 | $1\times1/1\times1$ | -4.14 |
| BL $MoS_2/Zr_2NF_2$ | 3.308 | -2.75 | $1\times1/1\times1$ | -3.74 |
| BL $MoS_2/Nb_2CO_2$ | 3.136 | 2.59 | $1\times1/1\times1$ | -6.07 |
| BL $MoS_2/Cr_2NO_2$ | 2.871 | -2.99 | $\sqrt{3}\times\sqrt{3}/2\times2$ | -7.01 |
| BL $MoS_2/Cr_2CO_2$ | 2.777 | 0.32 | $\sqrt{3}\times\sqrt{3}/2\times2$ | -7.09 |
| BL $MoS_2/Mo_2NO_2$ | 2.87 | -2.94 | $\sqrt{3}\times\sqrt{3}/2\times2$ | -6.02 |
| BL $MoS_2/Mo_2CO_2$ | 2.879 | -3.23 | $\sqrt{3}\times\sqrt{3}/2\times2$ | -7.67 |

**Table S2**. Energy differences between each stacking pattern and the most stable stacking pattern of the BL $MoS_2/Sc_2NF_2$ and BL $MoS_2/Sc_2NO_2$ vdW heterostructures. $d_v$ is the vertical distance between the two layers.

| Interface | Property | Atop-I | Atop-II | Fcc-I | Fcc-II | Hcp-I | Hcp-II |
|---|---|---|---|---|---|---|---|
| BL $MoS_2/Sc_2NF_2$ | $\triangle E$ (meV) | 0 | 7.77 | 113.17 | 113.41 | 18.82 | 12.62 |
| | $d_v$ (Å) | 2.47 | 2.53 | 3.06 | 3.06 | 2.57 | 2.52 |
| BL $MoS_2/Sc_2NO_2$ | $\triangle E$ (meV) | 0 | 19.97 | 135.80 | 142.16 | 33.71 | 2.95 |
| | $d_v$ (Å) | 2.41 | 2.49 | 2.86 | 2.88 | 2.56 | 2.44 |

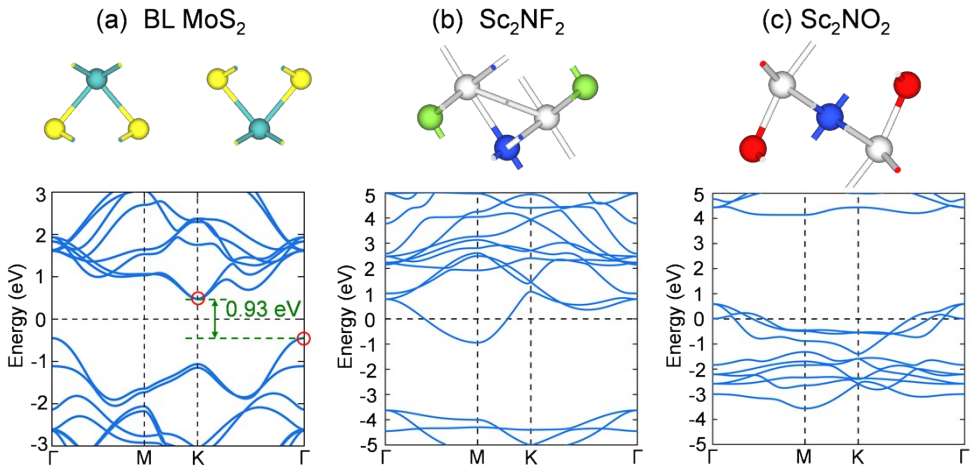


**Figure S1.** The geometric structures and band structures of (a) BL $MoS_2$, (b) ML $Sc_2NF_2$, and (c) ML $Sc_2NO_2$.

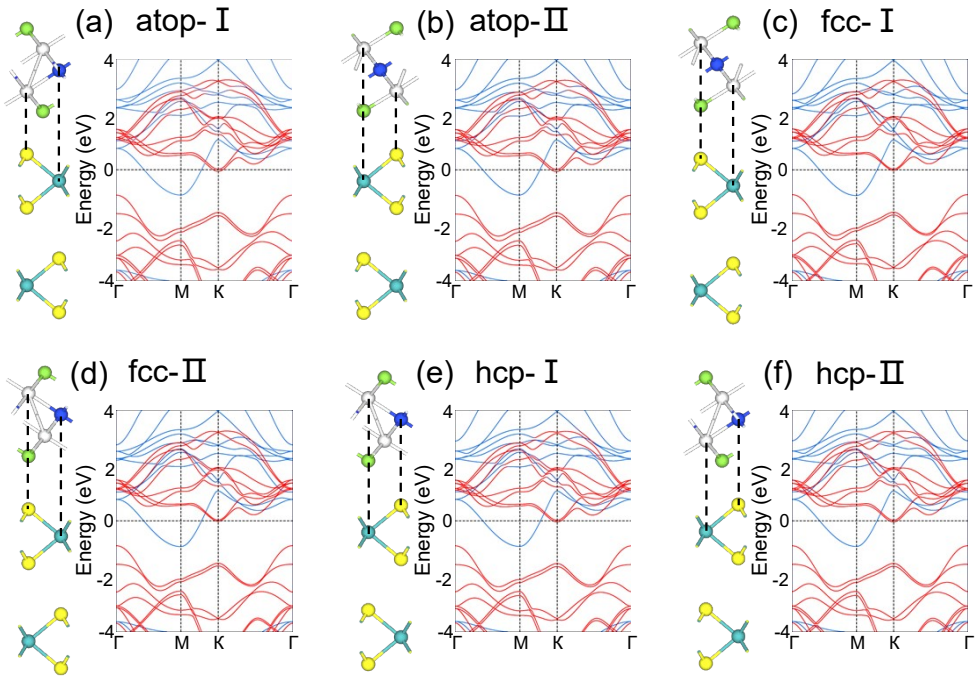


**Figure S2.** The stacking patterns and projected band structures of the BL $MoS_2/Sc_2NF_2$ vdW heterostructure. (a) Atop-I. (b) Atop-II. (c) Fcc-I. (d) Fcc-II. (e) Hcp-I. (f) Hcp-II.

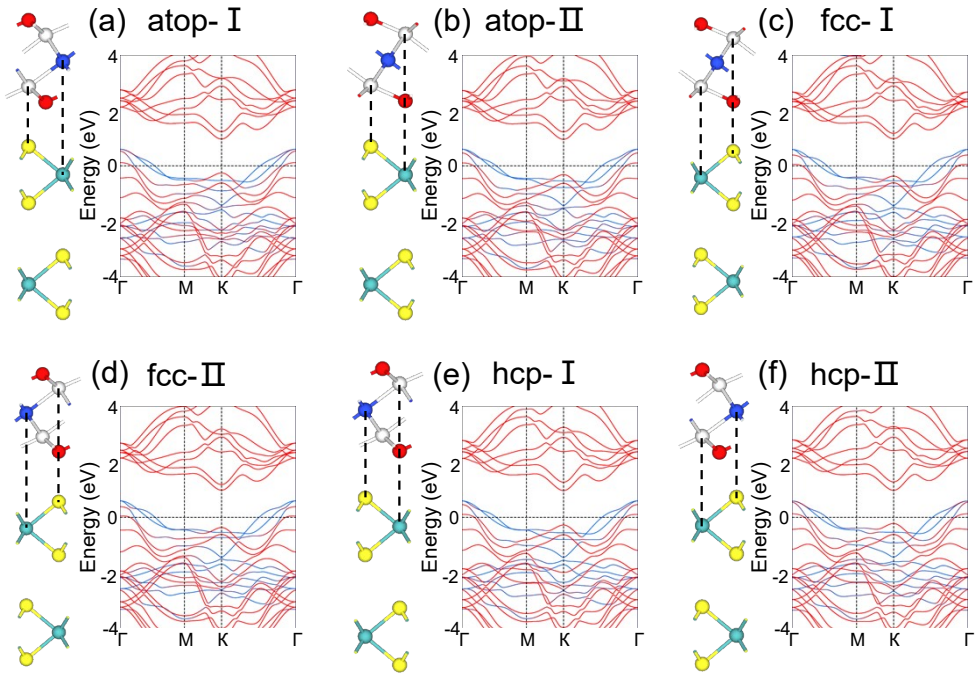


**Figure S3.** The stacking patterns and projected band structures of the BL $MoS_2/Sc_2NO_2$ vdW heterostructure. (a) Atop-I. (b) Atop-II. (c) Fcc-I. (d) Fcc-II. (e) Hcp-I. (f) Hcp-II.

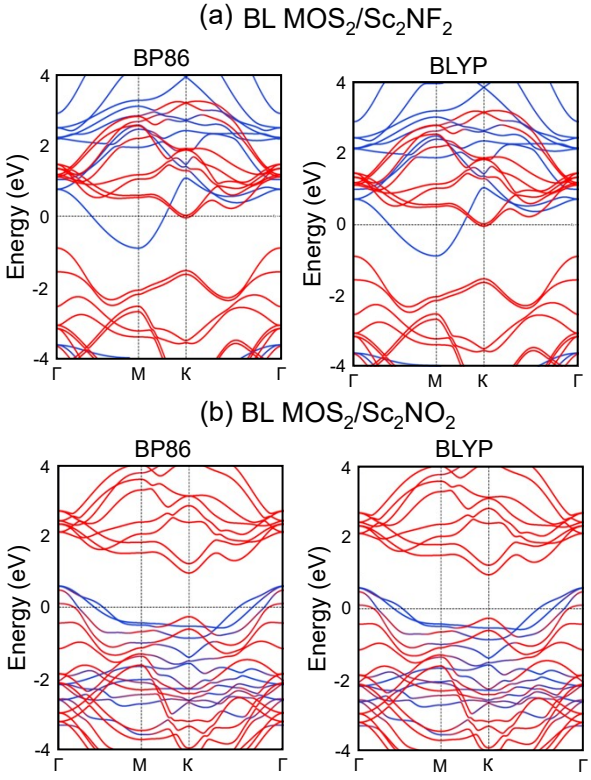


**Figure S4.** The projected band structures of (a-b) BL $MoS_2/Sc_2NF_2$ and (c-d) BL $MoS_2/Sc_2NO_2$ computed with GGA-BP86 and GGA-BLYP functionals.